10.1029/93JC01184

JOURNAL OF GEOPHYSICAL RESEARCH, VOL. 98, NO. C11, PAGES 20,121–20,131, NOVEMBER 15, 1993

Eddies in the North Brazil Current Retroflection Region Observed by Geosat Altimetry

NORBERT DIDDEN AND FRIEDRICH SCHOTT

Institut für Meereskunde an der Universität Kiel, Kiel, Germany

Mesoscale fluctuations in the western tropical Atlantic are analyzed in Geosat altimetry sea surface height (SSH) and geostrophic velocity anomalies to investigate the role of eddies in the North Brazil Current (NBC) retroflection zone. The detachment of anticyclonic eddies from the NBC retroflection is observed during November through January, when the NBC retroflection into the North Equatorial Countercurrent (NECC) weakens and finally breaks down. These eddies are traced over more than 2 months between 50° and 60°W on their way toward the Caribbean, at average speeds of 15 cm s^{-1}. In one case an apparent merger of two anticyclonic eddies occurs, one detached from the retroflection zone and one detached from the NECC. Cyclonic eddies are also observed but are generally less persistent. Mesoscale SSH variance just west of the retroflection increases by a factor of 2 from early summer to winter, mainly because of the anticyclonic eddies. Interhemispheric water mass transfer associated with the eddy flux out of the NBC retroflection may amount to an average transport of 3 Sv.

1. INTRODUCTION

The North Brazil Current (NBC) is a low-latitude western boundary current which carries water supplied by the South Equatorial Current from the tip of Brazil near 5°S northwestward along the coast and across the equator into the northern hemisphere. It is well established on the basis of historical ship drift data [*Richardson and Walsh*, 1986] and by analysis of satellite coastal zone color scanner (CZCS) data [*Müller-Karger et al.*, 1988] and Geosat altimetry [*Carton and Katz*, 1990; *Didden and Schott*, 1992, hereinafter referred to as DS] that during summer and fall the NBC surface flow separates from the coast and turns offshore at about 6°N to feed the eastward flowing North Equatorial Countercurrent (NECC). What happens during the other season is still a matter of debate. In late winter to spring, the NECC is weak or even flowing westward [*Richardson and Reverdin*, 1987; DS], while the cross-equatorial flow of the NBC does not significantly diminish from its summer value [*Schott et al.*, 1993]. The presumed consequence was enhanced northwestward flow parallel to the coast off Guiana in late winter to spring. This seasonal maximum was indeed observed north of the retroflection zone in Geosat-derived geostrophic surface currents [DS], but it appeared to taper off before reaching the Caribbean. Similarly, analysis of the surface circulation in the high-resolution numerical World Ocean Circulation Experiment Community Effort North Atlantic Model that was found to fairly realistically represent the general features of the surface circulation in the tropical Atlantic circulation does not yield a throughflow during late winter from south of the equator along the coast into the Caribbean [*Schott and Böning*, 1991; DS].

Yet, water masses of South Atlantic origin enter the eastern passages of the Caribbean and constitute a significant fraction of the Florida Current transport [*Tsuchiya*, 1989; *Schmitz and Richardson*, 1991]. One way to accomplish northwestward water mass transfer along the boundary is by eddy shedding from the NBC/NECC retroflection regime. Eddy detachment and water mass transfer are known from other retroflection regimes and have been reported, e.g., for the Agulhas by *Lutjeharms and Van Ballegooyen* [1988] and *Gordon and Haxby* [1990], for the South Madagascar retroflection zone by *Lutjeharms* [1988], and for the Leeuwin Current by *Church et al.* [1989]. For the NBC retroflection, *Johns et al.* [1990] evaluated CZCS images and moored current meter records and concluded that during the NBC retroflection phase in late summer and fall, anticyclonic eddies periodically break off from the retroflection region and drift along the Guiana coast toward the Caribbean.

In the present paper we use Geosat altimetry to investigate the mesoscale variability along the western boundary current from altimetric sea surface height (SSH) anomaly maps referenced to the 2-year mean SSH. The quality of mesoscale eddy detection by Geosat sampling and objective mapping is first explored in a simulation using Gaussian-shaped eddies. Between the NBC retroflection region and the Caribbean, westward propagating eddies are identified, and the translation of these eddies is followed over several months. In particular, the seasonal occurrence, scale, and translation speed of anticyclonic eddies originating from the NBC retroflection current loop are investigated. For verification, time series of geostrophic velocity fluctuations derived from the SSH anomaly maps are compared with simultaneous current meter records from a mooring near the retroflection region. We finally discuss the role of the eddies for interhemispheric water mass transfer.

2. ALTIMETER DATA AND EDDY SAMPLING

For mesoscale eddy detection we derived SSH anomalies (i.e., residuals relative to a 2-year mean sea surface) from Geosat Exact Repeat Mission altimeter data [*Cheney et al.*, 1987] for the period November 1986 through June 1989, using the collinear analysis method. We give only a short description of the procedure here and refer the reader to DS for details. The usual corrections supplied with the Geosat data were applied to the raw altimetric height measurements after editing for spurious data. For each ground track in the region 10°S to 30°N of the tropical Atlantic, the 2-year mean over 43 sea level profiles, sampled with a 17-day repeat

Paper number 93JC01184.
0148-0227/93/93JC-01184$05.00

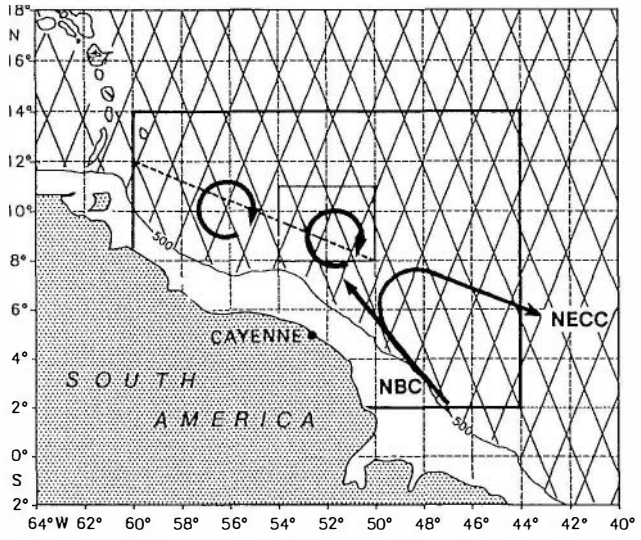

Fig. 1. Geosat tracks in the western tropical Atlantic Ocean. The North Brazil Current (NBC) retroflection into the North Equatorial Countercurrent (NECC) and eddies in the North Brazil Current extension are shown schematically. The broken line indicates the path of a model eddy used to study Geosat sampling characteristics. Also shown are the mapping region (outer box) and the region of seasonal variability displayed in Figure 8 (small interior box).

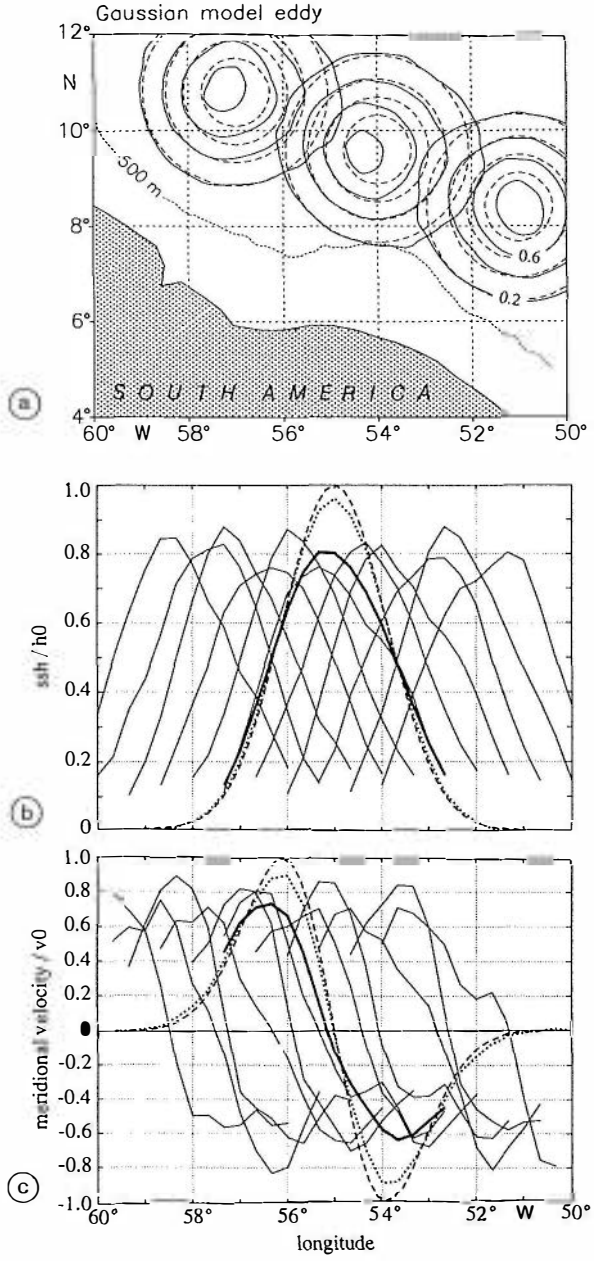

Fig. 2. Geosat-sampled and objectively analyzed data (solid lines) from a Gaussian model eddy (dashed lines), which propagates from 50° to 60°W in 90 days. (*a*) Sea surface height (SSH) contours (interval, 0.2) are selected from three maps 27 days apart. SSH profiles (*b*) and meridional velocity profiles (*c*) on zonal sections through the eddy center are shown every 6 days. Ensemble mean profiles (heavy solid lines) are arbitrarily shown centered on 55°W. Smoothing by objective analysis of a gridded (1/3°) model eddy (without Geosat sampling) is indicated by the dotted profile.

period, was subtracted from the individual SSH profiles for ocean depths exceeding 500 m. For the area of interest, tide correction errors in shallow water were discussed by DS and have been shown to be important at depths of less than 500 m only. Orbit errors were removed using quadratic polynomials least squares fitted over tracks, which in the NBC region west of 50°W are about 3000 km in length. The resulting along-track SSH anomaly profiles were median filtered over 70 km and subsampled at 20-km intervals.

The data distributed irregularly in space and time were interpolated onto a regular grid using the objective analysis method [*Bretherton et al.*, 1976] in a modified version suited for large data sets [*DeMey and Menard*, 1989]. For the extraction of the mesoscale surface topography, an isotropic correlation scale of 150 km and an exponential temporal correlation with a 15-day timescale were assumed. SSH anomaly maps with a resolution of 1/3° in latitude and longitude were computed every 3 days for the time period November 1986 through June 1989. From these maps, mesoscale features could be traced reasonably well as they moved across the Geosat track pattern shown in Figure 1.

In order to estimate the filter effects of Geosat sampling and objective mapping upon the amplitude of mesoscale eddy SSH signals, we performed tests by analyzing a Gaussian model eddy of radial SSH distribution $h = h_0 \exp(-\frac{1}{2}r^2/R_e^2)$, where R_e is the eddy radius of maximum (geostrophic) velocity. This model eddy was sampled along tracks corresponding to the original Geosat data coverage and objectively analyzed in the same way as the Geosat data.

For a model eddy of unit maximum height h_0 and radius R_e = 120 km propagating within 90 days with a speed of about 15 cm s^{-1} from 8°N, 50°W to 12°N, 60°W (dashed line of Figure 1), the SSH signal was analyzed every 3 days on a 1/3° by 1/3° grid. The size and propagation of this test eddy are typical for the eddies observed in this study. Figure 2 shows examples of the mapped model eddy and of zonal sections through the eddy center for SSH and meridional geostrophic velocity, both normalized with model profile maximum values. The analyzed profiles of the westward drifting model eddy are shown at 6-day intervals. The ensemble mean of these profiles (heavy solid line), averaged with respect to the instantaneous model eddy center, is shown for comparison with the Gaussian model eddy (dashed line), with both arbitrarily centered at 55°W. For all

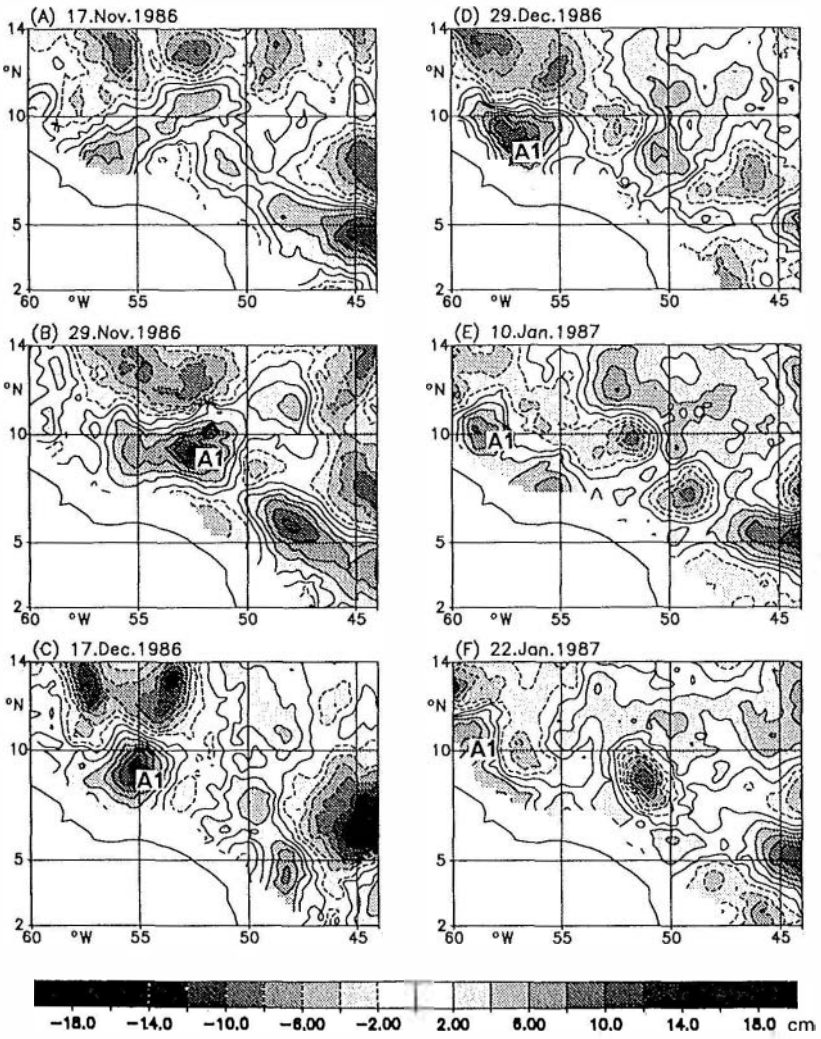

Fig. 3. SSH anomaly for November 1986 to January 1987 (contour interval, 2 cm). Time intervals between consecutive maps are 12 or 18 days. An anticyclonic eddy (A1) is observed to propagate westward. (*a*) November 17, (*b*) November 29, (*c*) December 12, (*d*) December 29, (*e*) January 10, and (*f*) January 22.

individual profiles of the 30 analyzed maps (eddy center, 50°–60°W), the maximum eddy height ranged from 0.72 to 0.91 h_0, and maximum swirl velocities ranged from 0.47 to 0.90 of maximum model eddy velocity. The ensemble mean profiles indicate a reduction of 20% (0.80 ± 0.05) for maximum SSH and of about 30% (0.69 ± 0.10) for maximum geostrophic swirl velocity. The radius defined by maximum velocity is increased by 12%. The same results were found in tests with model eddies propagating at a different phase relative to Geosat sampling: the ensemble mean SSH and swirl velocity profiles showed different asymmetries with respect to the eddy center but equal SSH maxima and equal averages over both velocity maxima. Most of the amplitude reduction is due to the coarse Geosat sampling. The objective mapping procedure by itself accounts for a decrease of only about 5% in maximum SSH and 10% in maximum velocity as inferred from objective analysis of synoptic gridded model eddy data rather than of Geosat subsampled data (Figure 2, dotted line). In addition to those factors, the quality of eddy detection depends on the eddy signal to noise ratio in the true Geosat data, which is discussed below.

3. Eddy Observations From SSH Anomaly Maps

Between 50° and 60°W, several events of westward propagating isolated positive SSH anomalies are identified (Figures 3 and 4). During December 1986 and January 1987, an anticyclonic eddy (named A1) is traced between 52° and 57°W along about 9°N latitude (Figures 3*a* to 3*d*). It then moves northwestward to 60°W, 11°N, following the orientation of the continental shelf break (Figures 3*e* to 3*f*). Its origin could be the NBC/NECC retroflection zone near 6°N, 49°W, where it appears to pinch off in mid-November (Figure 3*a*).

A similar sequence is observed 1 year later: during October 1987, the positive SSH anomaly centered at 51°W, 7°N (Figures 4*a* and 4*b*) is associated with the NBC retroflection and remains approximately fixed in space. In late November (Figure 4*c*), an eddy has separated from the westernmost edge of the NBC retroflection at 51°W and started propagating westward. This anticyclonic eddy (B1) moves westward in the 8°–10°N latitude range through early February 1988,

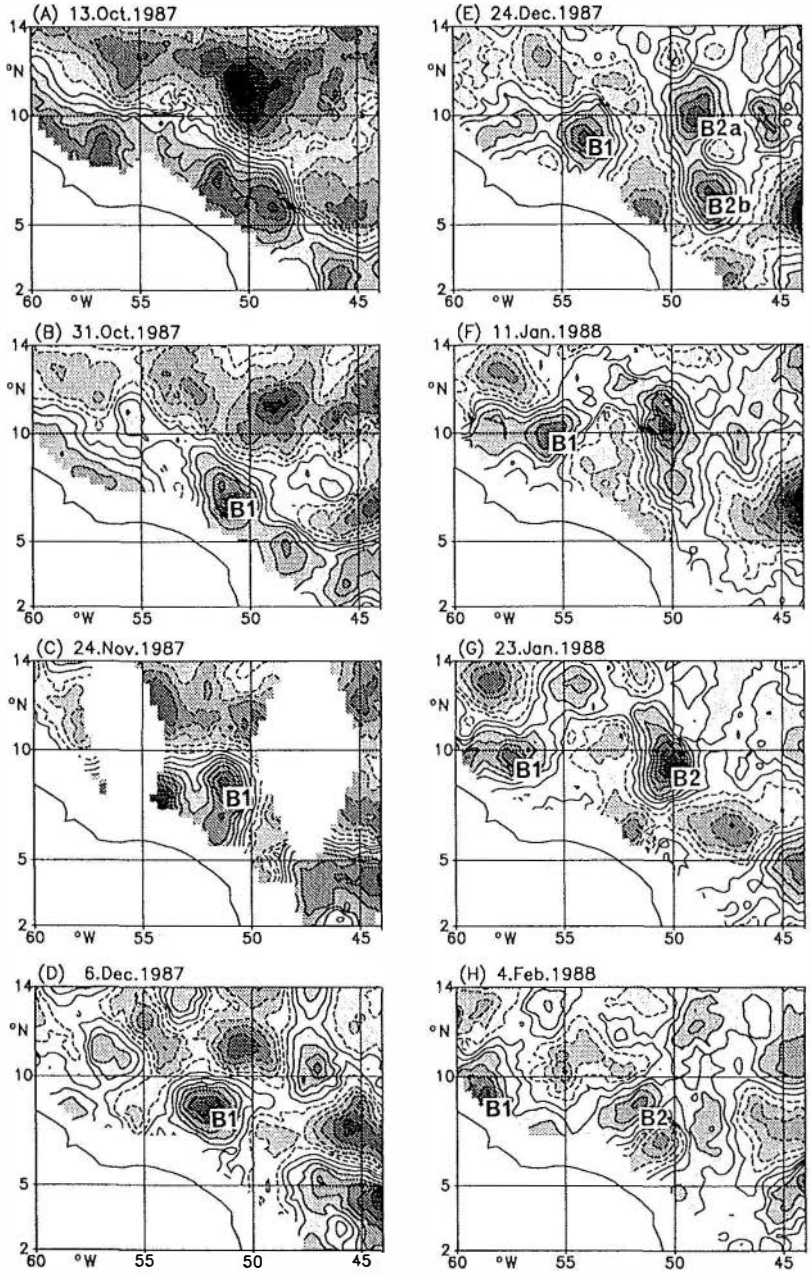

Fig. 4. SSH anomaly for October 1987 to May 1988 (contour interval, 2 cm; grey scales as in Figure 3). Westward propagating anticyclonic eddies (positive SSH anomaly) are (*a–h*) eddy B1, (*e–m*) eddy B2, and (*i–o*) eddy B3.

when it approaches the continental rise at 59°W, 9°N (Figures 4*d* to 4*h*).

The paths of two further anticylonic eddies are tracked in early 1988. About 60 days after eddy B1, a positive isolated SSH anomaly (B2) propagates from 50°W, 9°N to 59°W, 12°N (Figures 4*g* to 4*m*). During February and March, this eddy is detected in the 2-week intervals of Figures 3*h* to 3*l* with varying amplitude in longitude increments of roughly 2°. The origin of eddy B2 can be identified in the previous maps. It is formed from the merging of two positive SSH anomalies indicated in the map sequence of Figures 4*d* to 4*g*: a northern anticyclonic eddy (B2a) starts in early December from about 47°W, 10°N (Figure 4*d*), where it may have been generated in the shear zone between the North Equatorial Current and the decaying NECC. A southern anticyclonic eddy (B2b) is for the first time observed as an isolated positive SSH anomaly at 48°W, 6.5°N (Figure 4*e*); i.e., it originates from the NBC retroflection tongue, which in early December 1987 (Figure 4*d*), after the separation of eddy B1, extends westward to about 48°W. A third anticyclonic eddy (B3) during this winter season is observed about 30 days later: between February and early May, it moves westward from 49°W, 7°N to 59°W, 11°N (Figures 4*i* to 4*o*), again in increments of roughly 2° of longitude. The positive anomalies B2 and B3 are less well sampled than eddies A1 and B1: at some positions their shapes are more elongated and their amplitudes are lower than other extrema of the same maps. They are, however, clearly identified by their systematic westward propagation.

The quality of objective eddy mapping may be inferred

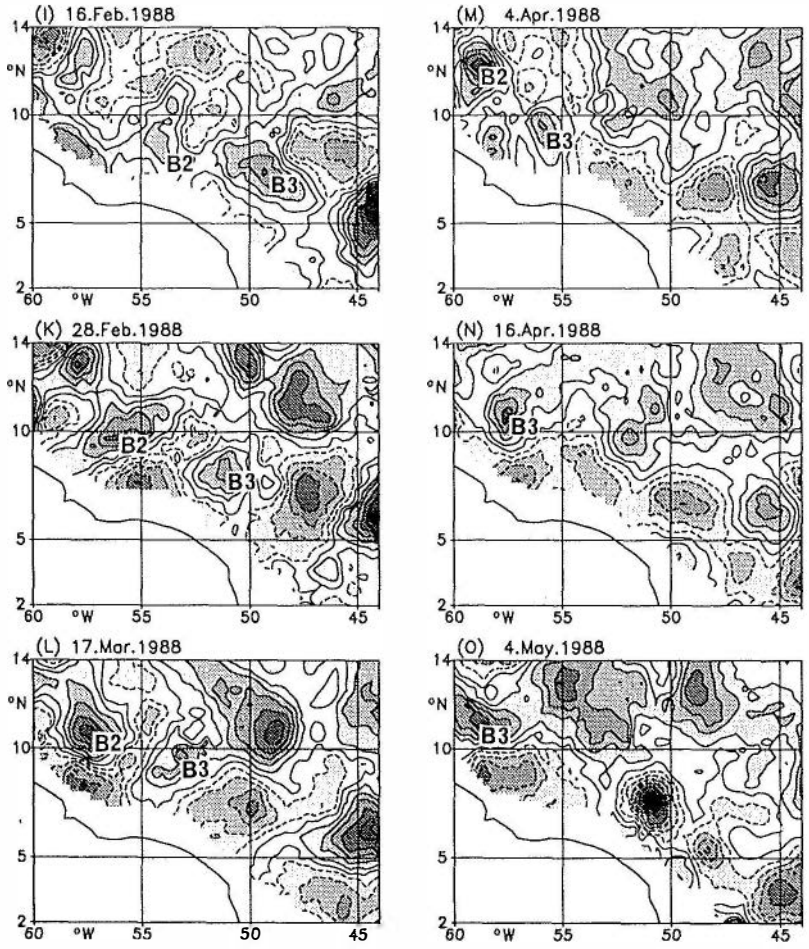

Fig. 4. (continued)

from comparison of alongtrack SSH signals with mapped data interpolated back to the Geosat tracks: some examples of tracks crossing the eddies A1 and B1 (not necessarily at the eddy center) are shown in Figure 5. The mapped data are taken from maps within 1.5 days of the satellite pass, where it has to be noted that the mapped signal is influenced by data from crossing satellite passes as well. The difference signal between along-track SSH and mapped SSH represents small-scale oceanic variability and altimeter noise. The root-mean-square difference is 2.1 cm, i.e., about 20% of the eddy amplitude of typically more than 10 cm. The reduction of maximum SSH gradients associated with the eddies in the along-track signal of Figure 5 is about 20% on average. This is less than the mean 30% resulting from our zonal sections across the model eddy (Figure 2*c*) and may be due to the better meridional sampling of the eddies by the Geosat ground tracks (Figures 1 and 2*a*).

The paths of the anticyclonic eddies in the winter seasons 1986–1987 (eddy A1) and 1987–1988 (eddies B1, B2, and B3) are summarized in Figure 6: the eddies roughly follow the continental shelf, as indicated by the 500-m depth contour. Propagation speeds are between 13 and 18 cm s^{-1} over a period of 1.5 to 2.5 months (Table 1). Eddies are first detected north or west of the NBC/NECC retroflection region and in cases A1 and B1 appear to break off from it after a preconditioning phase during which the retroflection

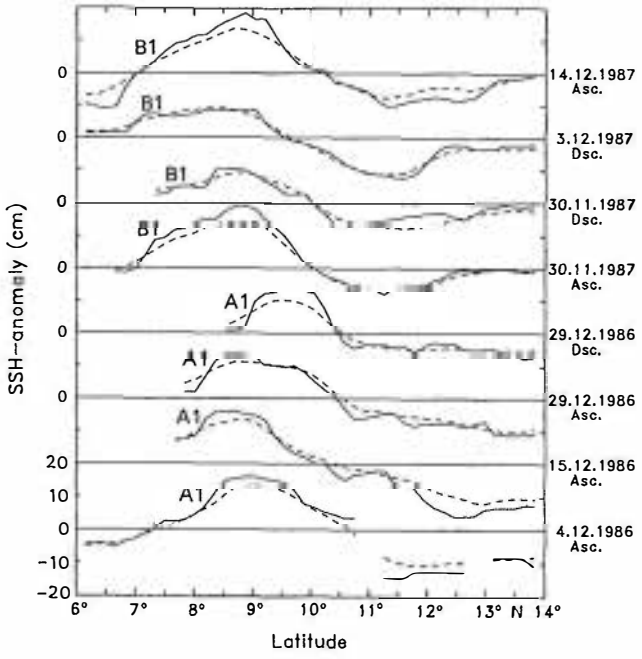

Fig. 5. SSH anomaly along selected tracks crossing eddies A1 and B1. Dashed lines show profiles after space-time objective mapping and interpolation to Geosat tracks. Time refers to ascending (Asc) or descending (Dsc) satellite passes. Offset is 20 cm.

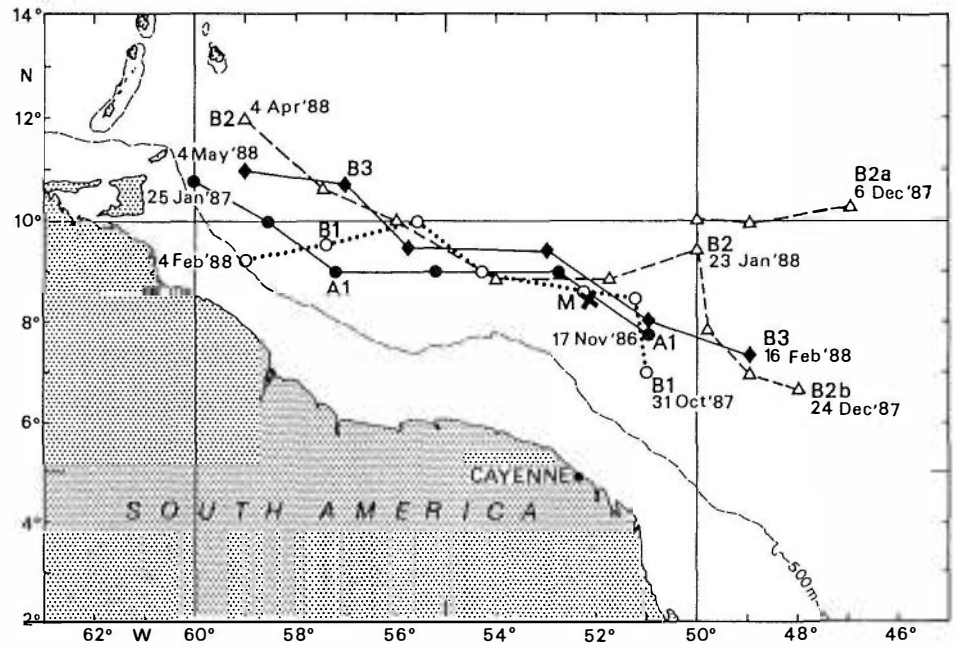

Fig. 6. Paths of anticyclonic eddy centers. Also shown is position of moored station (M) of *Johns et al.* [1990].

zone reaches up to 9°N (Figures 3*a* and 4*a*). After that, an eddy breaks off, leaving the retroflection behind it farther south.

From the SSH anomaly maps we estimated the eddy radius, which we define here as the distance from the eddy center to the point of half the maximum SSH anomaly value (noncircular SSH anomalies were averaged azimuthally). The radius of each anticyclonic eddy, averaged over the SSH maps displayed in Figures 3 and 4 is listed in Table 1; the typical eddy radius (for half the maximum amplitude) is 130 km.

4. Seasonal Distribution of Eddy Variability

The seasonal distribution of SSH anomalies is shown in the latitude-time plot of Figure 7: each box displays SSH contours in the 6°–14°N latitude range for data averaged over 1° in longitude. Features propagating westward along the northern Brazil and Guiana coasts are clearly identified from their time displacement in longitude. The dominant westward propagating positive SSH anomalies (Figure 7*a*) are the signatures of the anticyclonic eddies: one event in late 1986 (eddy A1) and three events in the fall–winter season of 1987–1988 (eddies B1 to B3). Despite the gappy altimeter sampling in late 1988 and 1989, at least one more anticyclonic eddy (C1) is observed to propagate from 50° to 60°W during January to April 1989. There are also weaker or more convoluted anomalies, some of which also appear to propagate westward, but only isolated eddies tracked over at least 5° in longitude are marked.

Larger patches of SSH anomalies in the latitude-time plots, having large zonal extensions as well, are associated with seasonal variations, e.g., the positive anomaly north of 10°N during March through June in 1987 and 1988 (Figure 7*a*). This ridge corresponds to the northern border of the seasonal maximum of westward NBC flow [DS]. It is associated with a 21 cm s^{-1} westward phase speed of the annual harmonic variation of SSH (fitted to the 1987–1988 2-year time series). Similarly, the region of high SSH in the latitude range 6°–9°N is associated with the seasonal slowdown of the NBC during August through November.

Some isolated negative SSH anomalies are also identified as propagating westward (Figure 7*b*). The cyclonic eddies seem to be less persistent; i.e., they can be traced over a zonal distance of only a few degrees, at most over 6°. One such eddy, originating near 6.5°N, 46°W (Figure 3*d*) and propagating westward (Figures 3*e* and 3*f*), is identifiable in Figure 3. Generally, the cyclonic eddies appear after the retroflection period and during the time when the western NECC is disorganized or westward flowing.

The SSH anomalies of Figure 7 suggest that the eddy

TABLE 1. Eddies in the NBC Region, 50°–60°W

Eddy	52°W Crossing Date	Propagation Velocity, cm s^{-1}	Longitude Range	Eddy Radius, km (Half Maximum SSH)
A1	Nov. 27, 1986	18	52.5°–58.5°W	140
B1	Dec. 6, 1987	13	51°–57.5°W	130
B2	Feb. 4, 1988	16	50°–57.5°W	115
B3	March 7, 1988	16	49°–59°W	120
C1	Feb. 16, 1989	16	50°–60°W	130

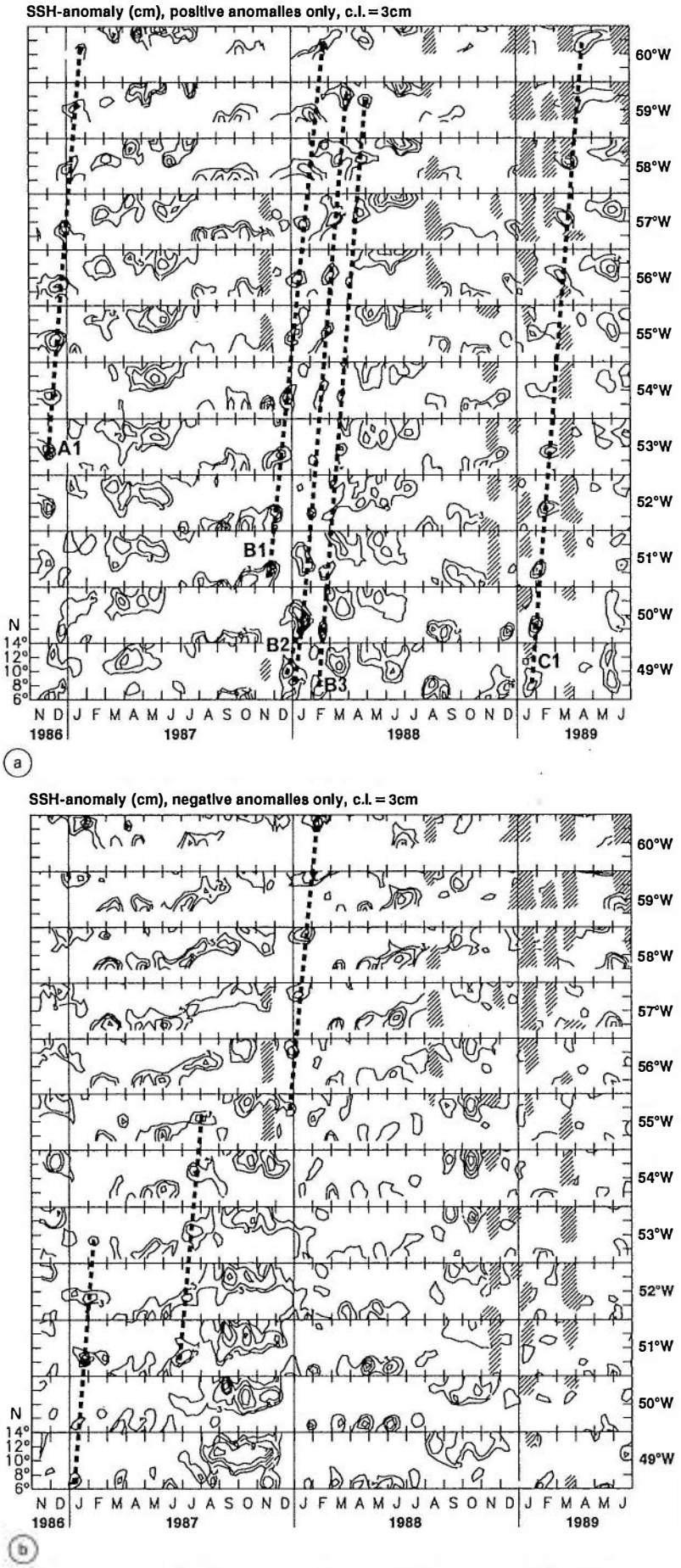

Fig. 7. Latitude-time plot of positive (*a*) and negative (*b*) SSH anomalies at longitudes 49° to 60°W (contour interval, 3 cm). The lines indicate phase propagation of those isolated SSH maxima and minima, which are tracked over more than 5° in longitude. Hatched areas indicate data gaps.

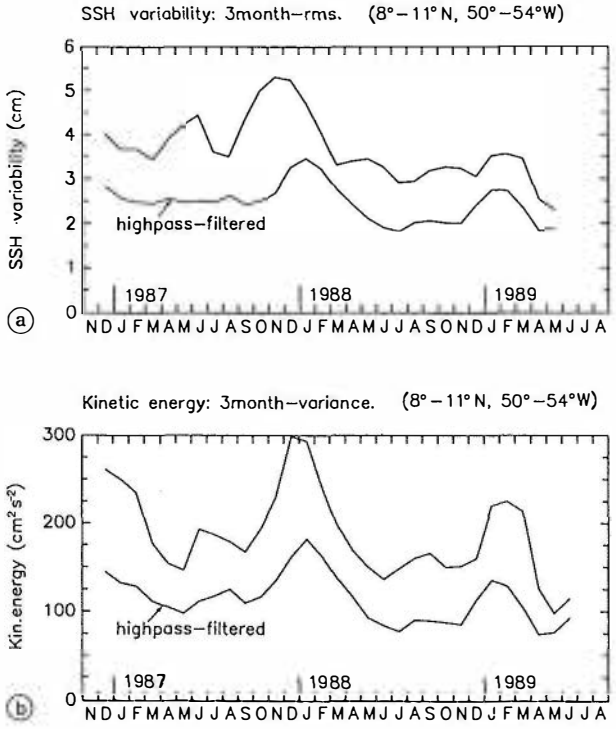

Fig. 8. Seasonal variation in the region 8°–11°N, 50°–54°W for (*a*) SSH root-mean-square (rms) variability and (*b*) geostrophic eddy kinetic energy (for moving 3-month averages). The lower curves show mesoscale eddy variability based on high-pass-filtered data (100 day cutoff period).

activity in the NBC extension region west of 50°W is strongest in the fall and winter seasons. The seasonal variations of SSH and of geostrophic current variability, computed for running 3-month means, are displayed in Figure 8 for the region 8°–11°N, 50°–54°W (Figure 1), i.e., just to the northwest of the NBC retroflection. Both the root-mean-square variability of SSH and the eddy kinetic energy $\frac{1}{2}(\overline{u'^2} + \overline{v'^2})$ of geostrophic velocity fluctuations (derived from the SSH anomaly maps, assuming geostrophic balance) show maxima in the November to February period and secondary maxima in summer. The total variability contains seasonal fluctuations as well as mesoscale eddy variability. The variability of high-pass-filtered time series (using a 100-day cutoff period) represents the mesoscale eddy activity with maxima centered in the winter months: the kinetic energy in January of 1988 and 1989 is increased by about 70% above the summer levels. Comparison of total and filtered variability shows that the secondary summer maxima are associated with the seasonal retroflection circulation.

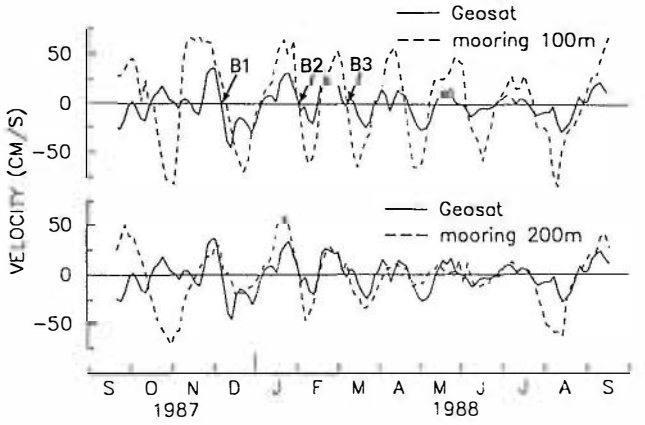

Fig. 9. Meridional velocity at 8.5°N, 52.1°W from Geosat (solid line) and from moored current meters [*Johns et al.*, 1990] at 100- and 200-m depths (dashed line). For this comparison the Geosat velocity is based on SSH maps, which were space-time interpolated assuming a westward propagation of 15 cm s^{-1} in the objective analysis (see text).

5. Eddy Velocity

The geostrophic velocity time series derived from the mapped altimeter SSH is compared with simultaneous 1-year-long current meter records at 100 and 200-m depths from a mooring at 52.15°W, 8.5°N (see Figure 6) near the NBC/NECC retroflection region (W. Johns and R. Zantopp, personal communication, 1991). In Figure 9 the anticyclonic eddies B1, B2, and B3 in December, February, and March, which are identified from altimetry (Figure 6), are clearly indicated by the strong meridional velocity fluctuations in the current meter data: anticyclonic eddy passage is associated with a change from positive to negative meridional velocity, and the zero-crossing time coincides well with the eddy passage time observed from altimetry (see also Table 1). The fluctuations of both data sets show smaller amplitudes during the summer period, in particular for the deeper velocities (200 m). The time series are generally well correlated except for the first period through mid-November 1987, when the strong fluctuations of current meter velocities are not in phase with the geostrophic surface velocity derived from Geosat. An explanation for this discrepancy is still lacking. The correlations of meridional velocity for the period starting in December 1987 are 0.69 for 100-m depth

TABLE 2. Meridional Velocity From Geosat Data and Moored Current Meters

	rms Amplitude, cm s^{-1}						
		Mooring		rms G/rms M		Correlation, G/M	
	Geosat	100 m	200 m	100 m	200 m	100 m	200 m
Sept. 1987–Sept. 1988	15.0	41.4	26.7	0.36	0.56	0.51	0.28
Dec. 1987–Sept. 1988	14.4	38.9	23.5	0.37	0.61	0.69	0.65
Dec. 1987–Sept. 1988	15.8	38.9	23.5	0.41	0.67	0.73	0.68

Current meters were at 8.5°N, 52.1°W. G, Geosat; M, mooring.
*Phase propagation $c_x = -15$ cm s^{-1} included in space-time interpolation of Geosat SSH anomaly.

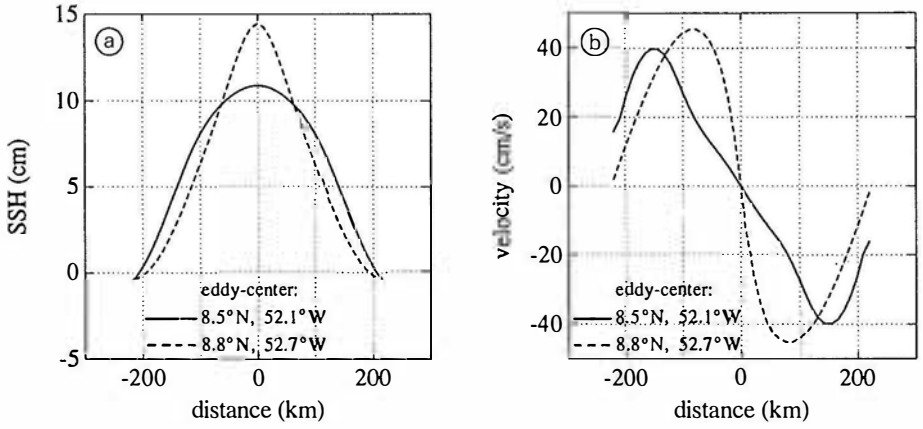

Fig. 10. (*a*) Axisymmetric SSH and (*b*) geostrophic velocity anomalies of eddy B1 at 8.5°N, 52.1°W (solid line) and 8.8°N, 52.7°W (dashed line).

and 0.65 for 200-m depth, i.e., considerably higher than for the full 1-year records (Table 2). The agreement is further improved if in the correlation function of the objective analysis procedure a westward phase speed of the Geosat-sampled SSH anomaly field is taken into consideration. In Figure 9 a westward propagation of 15 cm s^{-1} (typical eddy propagation speed; Table 1) for the comparison of the meridional velocity from Geosat and mooring data was used. The correlation between both velocities increases to 0.73 and 0.68 for the 100- and 200-m velocities, respectively (Table 2).

In Table 2 the ratios of root-mean-square velocity fluctuations determined from Geosat and measured by current meters are given. The smaller amplitudes of the Geosat-derived velocity fluctuations are partly expected as a consequence of the spatial filtering by Geosat sampling and objective analysis: a reduction of maximum geostrophic velocities of typically 30% was found in the analysis of test eddies using Geosat space-time coverage (Figure 2*c*). Another reason for the larger current meter velocity may be that the geostrophic balance is modified by the centrifugal force: the radial momentum balance for axisymmetric plane flow is

$$\frac{v^2}{r} + fv - g\frac{\partial h}{\partial r} = 0 \tag{1}$$

where v is the azimuthal velocity component. For anticyclonic eddies (i.e., $v < 0$), the Coriolis force has to balance the sum of the centrifugal and pressure gradient forces, both directed radially outward. The pressure gradient term can be substituted for by fv_g (derived from the geostrophic balance $fv_g = g\,\partial h/\partial r$) to obtain the relation

$$v_g = v\left(1 + \frac{v}{fr}\right) \tag{2}$$

between the geostrophic and total velocities. For an anticyclonic eddy of radius R_e, defined by the maximum velocity $-V_0$, the geostrophic velocity v_g underestimates the total velocity by a factor $1 - V_0/(fR_e)$. Conversely, solving (2) for v, the total velocity is obtained as a function of the measured altimeter geostrophic velocity. At radius $r = R_e$ of maximum geostrophic anticyclonic eddy velocity $-V_g$, this yields with $K = V_g/(fR_e)$:

$$\frac{V_0}{V_g} = K^{-1}\left[\tfrac{1}{2} - \left(\tfrac{1}{4} - K\right)^{1/2}\right] \tag{3}$$

From the SSH map of Figure 4*c* we have used zonal and meridional sections through the center of eddy B1 at 51°W, 8.5°N to estimate the axisymmetric approximation of the SSH distribution (Figure 10). A maximum geostrophic velocity of $V_g = 40$ cm s^{-1} at radius $R_e = 150$ km was obtained. According to (3), the total swirl velocity of this anticyclonic eddy is $1.17V_g$ ($K = 0.124$). Because of smoothing by Geosat sampling and mapping, the corrected geostrophic velocity may be $\hat{V}_g = 1.43V_g$ (for V_g being reduced by 30%) and the corrected radius may be 10% smaller (section 2), which leads to an eddy velocity of $V_0 = 1.37\hat{V}_g$ or $V_0 = 1.96V_g$; i.e., the Geosat-derived geostrophic velocity is only about 50% of the total eddy velocity. This explains most of the difference between the amplitudes of Geosat and current meter fluctuations (Table 2). From an SSH anomaly map from a few days later, when a Geosat track passed over the same eddy closer to its center (center position at 51.7°W, 8.8°N), the maximum SSH was 14 cm and the geostrophic velocity was $V_g = 45$ cm s^{-1} at radius $R_e = 90$ km (Figure 10). Owing to the considerably smaller eddy radius, the total velocity according to (1) is about 60% larger than the geostrophic velocity. This case with $K = 0.23$, however, is close to the case $V_g/(fR_e) < -0.25$, for which the anticyclonic eddy vorticity exceeds the planetary vorticity f and the steady momentum balance (1) is no longer possible.

In summary, the eddy observations from Geosat altimetry are consistent with direct local current measurements. Current fluctuations derived from altimetry are reduced against absolute currents by a factor of almost 2 owing to the combined effects of Geosat sampling, objective mapping, and the ageostrophic anticyclonic velocity component.

6. Interhemispheric Water Mass Exchange

The anticyclonic eddies can form a potentially important link in the interhemispheric water mass exchange. In winter

1986–1987, one eddy was found to break off, and it has to be considered that the Geosat coverage only began well into the season when breakoff can occur; in winter 1987–1988, three eddies were observed, and in winter 1988–1989, again one was observed, but at that time significant data gaps had already begun to occur. This count includes only eddies that could be clearly traced over at least 500 km. There are smaller, noisier signals that may also indicate water mass transfer out of the NBC/NECC retroflection. *Johns et al.*'s [1990] analysis of CZCS imagery from (fall to winter) 1979–1980 suggested the formation of three or four retroflection eddies during that year, similar to 1987–1988. The average radius of the five eddies traced in the Geosat analysis was 130 km (Table 1), but this was out to the average contour of half the maximum SSH anomaly in the center. The entire eddy radius is more like 200 km (Figure 10), in agreement with the estimates from CZCS imagery.

To reach a conclusion on water mass transfer by the anticyclonic eddies requires estimates of their vertical extent. The current meter analysis of *Johns et al.* [1990] shows the eddy signal, with decreasing amplitude, to reach deeper than 500 m. The float tracks of *Richardson and Schmitz* [1993] clearly showed the signature of anticyclonic eddies off the South American coast at the 800-m level. The measurements of the boundary current inflow into the retroflection zone by moored stations at 44°W across the NBC by *Schott et al.* [1993] showed the mean northwestward flow to decay from >100 cm s^{-1} near the surface to small values (<5 cm s^{-1}) at the 800-m level, and a ship section across the boundary current from July 1991 in that same study showed the warm-water transport to decay vertically to about 500-m depth. However, in an October 1990 ship section, the NBC was reaching to the 1000-m level with significant velocities. On the other hand, the vertical scale of the motion associated with the anticyclonic eddies may be larger than the actual water mass anomaly they carry. In water mass studies of Agulhas rings [*Olson and Evans*, 1986; *Gordon and Haxby*, 1990], the 10°C isotherm was used to define the bottom of the rings. In the retroflection region, latitude range 6°–8°N, the 10°C isotherm depth varies in the depth range of 300–400 m [*Colin et al.*, 1991].

Hence choosing a 10°C isotherm depth of 350 m as depth scale of the water mass anomalies carried by the eddies may yield a reasonable estimate, but water mass studies of retroflection eddies are required to advance in this subject. Based on an eddy radius of 200 km and a depth scale of 350 m, the volume for an individual eddy is 4.4×10^{13} m^3. At an average of two eddies detached per year, this amounts to a mean annual water mass transfer of 2.6 Sv. For three or four eddies generated as observed in 1979–1980 [*Johns et al.*, 1990] or in 1987–1988 in our Geosat analysis (Figure 7*a*), this number would go up to 3.9–5.2 Sv.

The anticyclonic eddies have been shown to propagate parallel to the continental slope (Figure 6) with an advection speed of about 15 cm s^{-1} (Figure 7*a*; Table 1). Thus the water mass transfer between the NBC/NECC retroflection region and the entrance of the Caribbean is accomplished within 2–3 months. This eddy translation speed is high compared with those derived from anticyclonic eddy observations based on the looping 800-m floats of *Richardson and Schmitz* [1993]. The mean advection speed for three anticyclonic eddies in the 50° to 59°W region is only 8.5 cm s^{-1}. Inspection of the individual float trajectories, however, shows the first float to be slow near 50°W and then to move to 52°W at 10.5 cm s^{-1} mean speed. The second float is trapped near 7°N, 50°W for about 2 months. Then, between early November 1989 and January 1990, it propagates to 59°W at a mean speed of about 14 cm s^{-1}. This eddy is similar to eddy B1 observed by altimetry at the sea surface 2 years earlier (Figures 4*a* to 4*c* and 7*a*): eddy B1 is also stagnant in the retroflection region during October 1987 before it separates in late November from the retroflection tongue and moves westward. For the third float the mean advection speed over 3.5 anticyclonic loops between 52° and 56°W is 20 cm s^{-1} before it slows down again. Using only those segments of the float tracks where the eddies progressed steadily while showing anticyclonic motion yielded a mean translation speed of 14.3 cm s^{-1}, in good agreement with the Geosat observations. *Johns et al.* [1990] estimated a drift of 10–15 cm s^{-1} for an eddy traced in CZCS images.

The fate of the anticyclonic eddies near the entrance of the Caribbean is not yet clear. Although some of them could be well traced to near the entrance of the Caribbean (Figure 6), Geosat altimetry on the western side of the Lesser Antilles did not provide evidence for the continued drift of the eddies into the Caribbean. One of the three 800-m eddy floats of *Richardson and Schmitz* [1993] wound up in the Grenada passage, and another one seemed to deflect northward before reaching the Antilles Arc at the time the float experiment ended.

The conveyer belt warm-water transfer, estimated at 13 Sv above 7°C [*Schmitz and McCartney*, 1993], occurs through the Caribbean, as shown by analysis of the water mass compositions of the Florida Current and Caribbean passages [*Schmitz and Richardson*, 1991]. At the deepest level of Carribean through flow, corresponding to the 7°C isotherm, the Subantarctic Intermediate Water is traced by its salinity minimum through the Caribbean to the bottom of the Straits of Florida [*Tsuchiya*, 1989].

The role the retroflection eddies play in relation to the mean flow regarding the composition of the water masses entering through the various passages of the Caribbean requires additional attention, both observational and modeling. In that respect it is interesting to note that present high-resolution numerical models, although reproducing the basic features of the near-surface circulation in the tropical Atlantic quite well [*Philander and Pacanowski*, 1986; *Schott and Böning*, 1991], do not produce detachment of isolated eddies that drift away from the NECC/NBC retroflection zone.

7. Summary and Conclusions

From SSH anomaly maps derived from the Geosat altimeter data for the period November 1987 to June 1989, we have observed the paths of several large anticyclonic eddies in the western boundary current of the equatorial Atlantic just north of the equator. These eddies are formed in the NBC retroflection region near 50°W at 6°–8°N, when the anticyclonic current loop of the NBC, which during late summer and fall leaves the coast and supplies water to the eastward flowing NECC, has its maximum northwestward extent and is in the process of breaking down. From the positive SSH anomaly signal, the eddies are tracked along the northern Brazil and Guiana coasts over a distance of about 1000 km. Cyclonic eddies were also found; they occur

after the breakdown of the retroflection and in the period of weak or westward flowing NECC. They are less frequent and could not be traced over as far as the anticyclonic eddies. The tracking simulation using Geosat sampling and analysis for an artificial Gaussian-shaped eddy with radius and propagation similar to those observed as well as comparison with moored current measurements of *Johns et al.* [1990] northwest of the retroflection zone showed that the mesoscale signals analyzed represented real eddies. However, because of the combined effects of Geosat track filtering, objective mapping, and ageostrophic velocity component, the Geosat-derived velocities are only about half the actual eddy velocities. While the year-long current measurements during 1987–1988 near the retroflection zone show energetic 40- to 60-day fluctuations throughout the year, with possibly a slight seasonal frequency modulation, only those of winter 1987–1988 are associated with eddies identifiable in the altimetry maps. The persistent 40- to 60-day background fluctuations seen in both current meter and altimeter measurements (with smaller amplitudes) appear to exist independently of the existence of the retroflection and need further explanation. It is plausible that the interaction of these background fluctuations with the retroflection causes the anticyclonic eddies to break off [*Johns et al.*, 1990].

Taking an average annual transfer of two anticyclonic eddies from the retroflection zone toward the Caribbean amounts to an annual mean water mass transfer of 3 Sv above 10°C, or about 20% of the North Atlantic thermohaline cell [*Schmitz and McCartney*, 1993] that carries heat from the southern to the northern hemisphere. *Johns et al.* [1990] produced an estimate of 4 Sv, assuming that a larger number of eddies (three or four) form each year but that they have smaller enclosed volumes, including only water above 200 m. Our estimate may be on the low side, since additional smaller eddy signals that could not be traced over longer distances but may add to this water mass transfer were also seen. It remains a deficiency of high-resolution numerical models, which otherwise appear to well represent the near-surface circulation of the tropical Atlantic [e.g., *Philander and Pacanowski*, 1986; *Schott and Böning*, 1991] that detachment of retroflection eddies and the associated water mass transfer are not sufficiently represented.

Acknowledgments. The collaboration of Detlef Stammer, IfM Kiel, in establishing the Geosat data analysis procedures is gratefully acknowledged. We also thank W. Johns and R. Zantopp of RSMAS, University of Miami, for providing the moored current meter data and P. Richardson of WHOI for providing 800-m float track data. W. Johns made helpful comments on an earlier version of the paper. This study has been supported by Deutsche Forschungsgemeinschaft, project SFB 133/A9.

REFERENCES

Bretherton, F., R. Davis, and C. Fandry, A technique for objective analysis and design of oceanographic experiments applied to MODE-73, *Deep Sea Res.*, *23*, 559–582, 1976.

Carton, J. A., and E. J. Katz, Estimates of the zonal slope and seasonal transport of the Atlantic North Equatorial Countercurrent, *J. Geophys. Res.*, *95*, 3091–3100, 1990.

Cheney, R. E., B. C. Douglas, R. W. Miller, D. L. Porter, and N. S. Doyle, Geosat altimeter geophysical data record user handbook, *NOAA Tech. Memo. NOS NGS-46*, Natl. Ocean Surv., Silver Spring, Md., 1987.

Church, J. A., G. R. Cresswell, and J. S. Godfrey, The Leeuwin Current, in *Poleward Flows Along Eastern Wave Boundaries*, edited by S. Neshyba et al., pp. 230–252, Springer-Verlag, New York, 1989.

Colin, C., R. Chuckla, B. Bourles, and P. Noyer, Programme NOE, Résultats hydrologiques et courantologiques des campagnes NOE (janvier, février, mars et octobre 1990), *Document scientifique O.P.III*, 76 pp., Centre ORSTOM de Cayenne, Cayenne, French Guiana, 1991.

DeMey, P., and Y. Ménard, Synoptic analysis and dynamical adjustment of GEOS 3 and Seasat altimeter eddy fields in the northwest Atlantic, *J. Geophys. Res.*, *94*, 6221–6230, 1989.

Didden, N., and F. Schott, Seasonal variations in the western tropical Atlantic: Surface circulation from Geosat altimetry and WOCE model results, *J. Geophys. Res.*, *97*, 3529–3541, 1992.

Gordon, A. L., and W. F. Haxby, Agulhas eddies invade the South Atlantic: Evidence from Geosat altimeter and shipboard conductivity-temperature-depth survey, *J. Geophys. Res.*, *95*, 3117–3125, 1990.

Johns, W. E., T. N. Lee, F. Schott, R. Zantopp, and R. Evans, The North Brazil Current retroflection: Seasonal structure and eddy variability, *J. Geophys. Res.*, *95*, 22,103–22,120, 1990.

Lutjeharms, J. R. E., Remote sensing corroboration of retroflection of the East Madagascar Current, *Deep Sea Res.*, *35*, 2045–2050, 1988.

Lutjeharms, J. R. E., and R. C. Van Ballegooyen, The retroflection of the Agulhas Current, *J. Phys. Oceanogr.*, *18*, 1570–1583, 1988.

Müller-Karger, F. E., C. R. McClain, and P. L. Richardson, The dispersal of the Amazon's water, *Nature*, *333*, 56–59, 1988.

Olson, D., and R. Evans, Rings of the Agulhas Current, *Deep Sea Res.*, *33*, 27–42, 1986.

Philander, G., and R. C. Pacanowski, A model of the seasonal cycle of the tropical Atlantic Ocean, *J. Geophys. Res.*, *91*, 14,192–14,206, 1986.

Richardson, P. L., and G. Reverdin, Seasonal cycle of velocity in the Atlantic North Equatorial Countercurrent measured by surface drifters, current meters, and ship drifts, *J. Geophys. Res.*, *92*, 3691–3708, 1987.

Richardson, P. L., and W. Schmitz, Deep cross-equatorial flow in the Atlantic measured with SOFAR floats, *J. Geophys. Res.*, *98*, 8371–8387, 1993.

Richardson, P. L., and D. Walsh, Mapping climatological seasonal variations of surface currents in the tropical Atlantic using ship drift data, *J. Geophys. Res.*, *91*, 10,537–10,550, 1986.

Schmitz, W. J., Jr., and M. McCartney, On the North Atlantic Circulation, *Rev. Geophys.*, *31*, 29–49, 1993.

Schmitz, W. J., Jr., and P. L. Richardson, On the sources of the Florida Current, *Deep Sea Res.*, *38*, suppl., S379–S409, 1991.

Schott, F., and C. W. Böning, The WOCE model in the western equatorial Atlantic: Upper-layer circulation, *J. Geophys. Res.*, *96*, 6993–7004, 1991.

Schott, F., J. Fischer, J. Reppin, and U. Send, On mean and seasonal currents and transports at the western boundary of the equatorial Atlantic, *J. Geophys. Res.*, *98*, 14,353–14,368, 1993.

Tsuchiya, M., Circulation of the Antarctic Intermediate Water in the North Atlantic Ocean, *J. Mar. Res.*, *47*, 747–755, 1989.

N. Didden and F. Schott, Institut für Meereskunde an der Universität Kiel, Düsternbrooker Weg 20, D-24105 Kiel, Germany.

(Received August 3, 1992;
revised April 28, 1993;
accepted April 28, 1993.)